



ISSN: 0067-2904

## Computational Analysis of Metallic- Nonmetallic Nanoparticle on Jeffery Hamel Nanofluid Flow Problem

Saja Issam Abdulridah, Abeer Majeed Jasim\*

Department of Mathematics, College of Science, University of Basrah, Basrah, Iraq

Received: 28/9/2022 Accepted: 29/1/2023 Published: 30/12/2023

### Abstract:

In this article, we investigate the heat transfer on nanoparticles Jeffrey Hamel flow problem between two rigid plane walls. Water is used as a main fluid using four different types of nanoparticles, namely aluminum, cuprous, titanium, and silver. The results of nonlinear transformational equations with boundary conditions are solved analytically and numerically. The perturbation iteration scheme (PIS) is used for the analytic solution, while for determining the numerical results, the Rang-Kutta of the four-order scheme (RK4S) is used. The effects on the behavior of non-dimensional velocity and temperature distributions are presented in the form of tables and graphs for different values of emerging physical parameters (Reynolds number, Prandtl number, Eckert number and open angles). The solid component of nanoparticles has an influence on the heat transfer and flow characteristics that is more visible when compared to other types of particles. The temperature distribution increases with the increase of the Reynolds number, Bruntel number, Eckert number, but the velocity distribution decreases with the increase of the Reynolds number. Finally, the obtained findings demonstrate PIS efficacy, accuracy, and convenience in solving the problem of nanofluid flow.

**Keyword:** Jeffrey Hamel, Magneto hydrodynamics, Nanofluid flow, Nanoparticles, Non-Parallel plates, Perturbation iteration scheme.

## التحليل الحسابي للجسيمات النانوية المعدنية غير المعدنية على مشكلة تدفق المائع النانوي لجيفري هامل

سجى عصام عبد الرضا ، عبير مجيد جاسم\*  
\*جامعة البصرة ، كلية العلوم ، قسم الرياضيات.

### الخلاصة:

تبحث الدراسة في هذه المقالة في مشكلة تدفق الحرارة على الجسيمات النانوية لجيفري هامل بين جدارين مستويين صليبين . يستخدم الماء كسائل رئيسي بإستخدام أربعة أنواع مختلفة من الجسيمات النانوية : الألمنيوم ، النحاس ، التيتانيوم والفضة. يتم حل نتائج المعادلات التحويلية غير الخطية بشروط حدودية تحليلياً وعددياً ، مع إكتشاف الحل التحليلي بإستخدام مخطط الاضطراب التكراري مع تحديد النتائج متضمناً مخطط رانج\_كوتا من الرتبة الرابعة التأثيرات على سلوك توزيعات السرعة غير الأبعاد ودرجة الحرارة في شكل جداول ورسوم بيانية لقيم مختلفة من المعلمات الفيزيائية الناشئة (رقم رينولدز ، رقم برانتل ، رقم إيكرت والزوايا المفتوحة). التأثير

\*Email: [saja.issam2@gmail.com](mailto:saja.issam2@gmail.com)

على نقل الحرارة وخصائص التدفق التي تكون أكثر وضوحًا عند مقارنتها بأنواع الجسيمات الأخرى. يزداد توزيع درجة الحرارة مع زيادة رقم رينولدز ورقم برنتل ورقم إيكرت ، لكن توزيع السرعة يتناقص مع زيادة رقم رينولدز. أخيرًا ، توضح النتائج التي تم الحصول عليها فعالية الطريقة ودقتها في حل مشكلة تدفق السوائل النانوية.

## 1. Introduction:

The presented manuscript deals with the study of the nanoparticles, their behavior, and the way they flow in different conditions by examining the changes that occur in each of the speed and temperature profiles when changing physical parameters and looking at the changes that occur. Nanofluid can be employed in a variety of technical applications in many industries, including electricity, and transportation, it relies on fluid heating and cooling. The cooling of any type of high energy gadget requires effective cooling solutions because of their poor heat transfer qualities. These qualities are commonly used to heat transfer fluids including water, ethylene glycol, and motor oil which have restricted heat transfer properties. The heat conductivities of metals can be up to three times greater than fluids, therefore the combining of two different compounds forms a heat transfer medium that behaves like a fluid, but it possesses the thermal conductivity of a metal which is naturally attractive. Jeffery and Hamel [1] were the most notable scientists who worked on nanofluid that involved the flow of incompressible nanofluid via mathematically diverging and converging channels. Recently, there are a significant, effective, and rising interest in nanofluidic analytical research. The solution to the Jeffery-Hamel flow problem is additional strategies. Nanofluid researcher Choi [2] was the first to use the term nanofluid. Bachok and Ishak [3] investigated the numerical heat transmission and flow properties pertaining to a nanofluid across a moving plate and they discovered that including nanoparticles in the base of fluid water increases friction coefficient and Nusselt number and thermal conduction. Kuznetsov and Nield [4] studied the effect of nanoparticles on the flow of a natural convection boundary layer through a vertical plate by taking Brownian motion and thermophoresis into account. Nadeem et al [5] studied solutions for the boundary layer flow in the vicinity of the stagnation point towards a stretched sheet. Rana and Bhargava [6] studied the effect of Brownian motion and thermophoresis on the natural convection of a nanofluid across a nonlinear sheet stretches by means of numerical methods. Moradi [7] investigated the heat transfer and viscous dissipation effects on the Jeffery-Hamel nanofluids. Many analytical approaches [8]- [30] have been created in recent years to tackle the majority of the scientific problem and phenomena faced in solving nonlinear ordinary differential equations. One of these approaches is the perturbation iterative scheme (PIS) [9], [10], [23] which has recently been used to solve many kinds of nonlinear problems [26]. In this study, a perturbation iterative scheme has been applied to find approximate analytical solutions to the nonlinear differential problems that govern Jeffrey-Hamel flow regarding heat transfer and viscous dissipation in nanofluids. The effect of active parameters such as nanoparticle volume fraction, opening angle, Reynolds number, Prandtl number and Eckert number on velocity and temperature boundary layer thicknesses [31] have been examined [24]. Analytical approximate solutions are given and compared with Runge-Kutta of fourth order scheme (RK4S), Differential Transformation method (DTM) [7], Homotopy Perturbation method (HPM) [8], Optimal Homotopy Asymptotic method (OHAM) [9], Spectral-Homotopy Analysis method (SHAM) [10], and Homotopy Analysis method (HAM) [11]. The results of the aforementioned are displayed in the tables and graphics. It can be said that the perturbation iteration scheme (PIS) is a simplified and acceptable method to reach approximate analytical solutions which are very similar to the most of methods that are used in the previous literature. In addition, this method has not been previously worked on nanoparticles in the Jeffrey Hamel equation, however, it met with approval and wide agreement.

**2. Mathematical formulation:**

Consider two-dimensional incompressible conductive viscous nanofluids flow between two rigid plane walls that meet at an angle of  $2\gamma$ . The water is the base fluid that contains several types of nanoparticles, namely Cu,  $Al_2O_3$ , Ag, and  $TiO_2$ . The velocity is completely radial and relies on  $r$  and  $\theta$ , so that  $V = (\tilde{u}(r, \theta), 0)$ . It is possible to describe the Jeffery-Hamel problem and the method of fluid flow on parallel walls geometrically as in Figure 1. The problem contains continuity, motion, and energy equations by taking the viscous dissipation. The statements of governing equations are defined as follows [8]:

$$\frac{\rho}{r} \frac{\partial(r\tilde{u})}{\partial r} (r\tilde{u}(r, \theta)) = 0 \quad , \tag{1}$$

$$\tilde{u} \frac{\partial \tilde{u}}{\partial r} = \frac{-1}{\rho_{n.f}} \frac{\partial P}{\partial r} - \frac{\mu_{n.f}}{\rho_{n.f}} \left[ \frac{\partial^2 \tilde{u}}{\partial r^2} - \frac{1}{r} \frac{\partial \tilde{u}}{\partial r} - \frac{1}{r^2} \frac{\partial^2 \tilde{u}}{\partial \theta^2} + \frac{\tilde{u}}{r^2} \right] \quad , \tag{2}$$

$$\frac{1}{\rho_{n.f} r} \frac{\partial P}{\partial \theta} - \frac{2\mu_{n.f}}{\rho_{n.f} r^2} \frac{\partial \tilde{u}}{\partial \theta} = 0 \quad , \tag{3}$$

$$\tilde{u} \frac{\partial T}{\partial r} = \alpha_{n.f} \left[ \frac{\partial^2 T}{\partial r^2} + \frac{1}{r} \frac{\partial T}{\partial r} + \frac{1}{r^2} \frac{\partial^2 T}{\partial \theta^2} \right] + \frac{\mu_{n.f}}{(\rho c_p)_{n.f}} \left[ 4 \left( \frac{\partial \tilde{u}}{\partial r} \right)^2 + \frac{1}{r^2} \left( \frac{\partial \tilde{u}}{\partial \theta} \right)^2 \right] \quad . \tag{4}$$

Where  $\tilde{u}$  is the velocity in the radial direction,  $P$  is the fluid pressure,  $\rho_{n.f}$  denotes the nanofluid viscosity coefficient density, and  $\alpha_{n.f}$  is the thermal diffusivity. The dynamic viscosity that is effective  $\mu_{n.f}$  and the effective density is  $\rho_{n.f}$ , the nanofluid is calculated as follows:

- $\rho_{n.f} = (1 - \varphi)\rho_f + \varphi\rho_s \quad ,$
- $\mu_{n.f} = \frac{\mu_f}{(1-\varphi)^{2.5}} \quad ,$
- $(\rho C_p)_{n.f} = (1 - \varphi)(\rho C)_f + \varphi(\rho C)_s \quad ,$
- $\alpha_{n.f} = \frac{K_{n.f}}{K_f} \quad ,$
- $\frac{K_{n.f}}{K_f} = \frac{(K_s + 2K_f) - 2\varphi(K_f - K_s)}{(K_s + 2K_f) + 2\varphi(K_f - K_s)}$  (5)

The solid volume fraction of nanofluid is denoted by  $\varphi$ ,  $(\rho C_p)_{n.f}$  is the heat capacity of the nanofluid, where  $(\rho C_p)_f$  and  $(\rho C_p)_s$  is the heat capacity of the base fluid and the solid fractional, respectively,  $K_{n.f}$  is the thermal conductivity of the nanofluid,  $K_f$  and  $K_s$  are the thermal conductivity of the base fluid and the solid of fraction, respectively. The  $\rho_f$  and  $\rho_s$  are the densities of the base fluid and the solid fractions, respectively. If  $u_\theta = 0$  for purely radial flow, the velocity parameter can get from Eq.(1) by product both sides by  $\left(\frac{r}{\rho}\right) \neq 0$  and then integration for  $r$  and put the integration constant for  $\theta$ :

$$\frac{\partial(r\tilde{u})}{\partial r} (r\tilde{u}) = 0, \quad r\tilde{u}(r, \theta) = h(\theta). \tag{6}$$

Also, derivative Eqs. (2) and (3) with respect to  $\theta$  and  $r$ , respectively. We get:

$$\frac{\tilde{u}(\partial^2 \tilde{u})}{\partial r \partial \theta} + \frac{\partial \tilde{u}}{\partial r} \frac{\partial \tilde{u}}{\partial \theta} = -\frac{1}{\rho_{n.f}} \frac{\partial^2 P}{\partial r \partial \theta} + \frac{\mu_{n.f}}{\rho_{n.f}} \left[ \frac{\partial^3 \tilde{u}}{\partial r^2 \partial \theta} - \frac{1}{r} \frac{\partial^2 \tilde{u}}{\partial r \partial \theta} - \frac{1}{r^2} \frac{\partial^3 \tilde{u}}{\partial \theta^3} + \frac{1}{r^2} \frac{\partial \tilde{u}}{\partial \theta} \right], \tag{7}$$

$$\frac{1}{\rho_{n.f} r} \frac{\partial^2 P}{\partial r \partial \theta} - \frac{1}{\rho_{n.f} r^2} \frac{\partial P}{\partial \theta} - \frac{2\mu_{n.f}}{\rho_{n.f} r^2} \frac{\partial^2 \tilde{u}}{\partial r \partial \theta} + \frac{4\mu_{n.f}}{\rho_{n.f} r^3} \frac{\partial \tilde{u}}{\partial \theta} = 0 \quad . \tag{8}$$

After arrangement Eqs. (7) and (8) by adding the following equation which is given as:

$$\frac{\tilde{u}(\partial^2 \tilde{u})}{\partial r \partial \theta} + \frac{\partial \tilde{u}}{\partial r} \frac{\partial \tilde{u}}{\partial \theta} = \frac{\mu_{n.f}}{\rho_{n.f}} \left[ \frac{\partial^3 \tilde{u}}{\partial r^2 \partial \theta} - \frac{1}{r} \frac{\partial^2 \tilde{u}}{\partial r \partial \theta} + \frac{1}{r^2} \frac{\partial^3 \tilde{u}}{\partial \theta^3} + \frac{\partial \tilde{u}}{\partial \theta} \right], \tag{9}$$

Since:

$$\hbar(\kappa) = \frac{\hbar(\theta)}{u_c}, \quad \tilde{u}(r, \theta) = \frac{u_c}{r} \hbar(\kappa), \quad \kappa = \frac{\theta}{\gamma}, \tag{10}$$

also,

$$\frac{T}{T_w} = \Theta(\kappa), \quad T(r, \theta) = T_w \Theta(\kappa). \tag{11}$$

Now, find the partial derivative of Eqs (9) and (4) by using Eqs. (10) and (11):

$$\begin{aligned} \frac{\partial \tilde{u}}{\partial \theta} &= \frac{u_c}{\gamma r} \left( \frac{d\hbar(\kappa)}{d\kappa} \right) & \frac{\partial^2 \tilde{u}}{\partial \theta^2} &= \frac{u_c}{\gamma^2 r} \left( \frac{d^2 \hbar(\kappa)}{d\kappa^2} \right) & \frac{\partial^3 \tilde{u}}{\partial \theta^3} &= \frac{u_c}{\gamma^3 r} \left( \frac{d^3 \hbar(\kappa)}{d\kappa^3} \right) \\ \frac{\partial^2 \tilde{u}}{\partial r \partial \theta} &= \frac{-u_c}{\gamma r^2} \left( \frac{d\hbar(\kappa)}{d\kappa} \right) & \frac{\partial \tilde{u}}{\partial r} &= \frac{-u_c}{r^2} \hbar(\kappa) & \frac{\partial^2 \tilde{u}}{\partial r^2} &= \frac{2u_c}{r^3} \hbar(\kappa) \\ \frac{\partial^3 \tilde{u}}{\partial r^2 \partial \theta} &= \frac{2u_c}{\gamma r^3} \left( \frac{d\hbar(\kappa)}{d\kappa} \right) & \frac{\partial T}{\partial r} &= 0 & \frac{\partial T}{\partial \theta} &= \frac{T_w}{\gamma} \left( \frac{d\Theta(\kappa)}{d\kappa} \right) \\ \frac{\partial^2 T}{\partial \theta^2} &= \frac{T_w}{\gamma^2} \left( \frac{d^2 \Theta(\kappa)}{d\kappa^2} \right) & \frac{\partial^2 T}{\partial r^2} &= 0. \end{aligned} \tag{12}$$

Substituting Eq. (10) into Eqs (9) and (4), we get

$$\begin{aligned} \frac{u_c}{r} \hbar(\kappa) \frac{-u_c}{\gamma r^2} \frac{d\hbar(\kappa)}{d\kappa} + \frac{-u_c}{r^2} \hbar(\kappa) \frac{u_c}{\gamma r} \frac{d\hbar(\kappa)}{d\kappa} &= \frac{\mu_{n.f}}{\rho_{n.f}} \left[ \frac{2u_c}{\gamma r^3} \frac{d\hbar(\kappa)}{d\kappa} - \frac{1}{r} \left( \frac{-u_c}{\gamma r^2} \frac{d\hbar(\kappa)}{d\kappa} \right) + \right. \\ &\quad \left. \frac{1}{r^2} \frac{u_c}{\gamma^3 r} \frac{d^3 \hbar(\kappa)}{d\kappa^3} + \frac{1}{r^2} \frac{u_c}{\gamma r} \frac{d\hbar(\kappa)}{d\kappa} \right], \end{aligned} \tag{13}$$

after simplifying the last equation ,we get:

$$-\frac{2u_c^2}{\gamma r^3} \hbar(\kappa) \frac{d\hbar(\kappa)}{d\kappa} = \frac{\mu_{n.f}}{\rho_{n.f}} \left[ \frac{4u_c}{\gamma r^3} \frac{d\hbar(\kappa)}{d\kappa} + \frac{u_c}{\gamma^3 r^3} \frac{d^3 \hbar(\kappa)}{d\kappa^3} \right]. \tag{14}$$

Now, product both sides by  $\left( \frac{\gamma^3 r^3}{u_c \rho_{n.f}} \neq 0 \right)$  and by using Eq. (5) to get the following:

$$\frac{d^3 \hbar(\kappa)}{d\kappa^3} + 2\gamma^2 \Re((1 - \varphi) + \varphi \frac{\rho_s}{\rho_f})(1 - \varphi)^{2.5} \hbar(\kappa) \frac{d\hbar(\kappa)}{d\kappa} + 4\gamma^2 \frac{d\hbar(\kappa)}{d\kappa}. \tag{15}$$

Also, from Eq. (4) and by substituting equation (12), this yields:

$$\left( \frac{u_c}{r} \hbar(\kappa) \cdot 0 \right) = \alpha_{n.f} \left[ 0 + 0 + \frac{T_w}{\gamma^2 r^2} \frac{d^2 \Theta(\kappa)}{d\kappa^2} \right] + \frac{\mu_{n.f}}{(\rho C_p)_{n.f}} \left[ 4 \frac{u_c^2}{r^4} (\hbar(\kappa))^2 + \frac{u_c^2}{\gamma^2 r^4} \left( \frac{d\hbar(\kappa)}{d\kappa} \right)^2 \right], \tag{16}$$

by using Eq.(5),

$$\alpha_{n.f} \frac{d^2 \Theta(\kappa)}{d\kappa^2} = \frac{\mu_{n.f}}{(\rho C_p)_{n.f} T_w r^2} \left[ 4\gamma^2 (\hbar(\kappa))^2 + \left( \frac{d\hbar(\kappa)}{d\kappa} \right)^2 \right]. \tag{17}$$

Therefore, Eqs (17) becomes as follows:

$$\frac{1}{[(1-\varphi) + \varphi \frac{(\rho C_p)_s}{(\rho C_p)_f}] \left[ \frac{K_{n.f}}{K_f} \frac{d^2 \Theta(\kappa)}{d\kappa^2} + \frac{P_r E_c}{(1-\varphi)^{2.5}} (4\gamma^2 (\hbar(\kappa))^2 + \left( \frac{d\hbar(\kappa)}{d\kappa} \right)^2) \right]} = 0, \tag{18}$$

with the following boundary conditions

$$\hbar(0) = 1, \quad \frac{d\hbar(0)}{d\kappa} = 0, \quad \hbar(1) = 0, \quad \Theta(1) = 1, \quad \frac{d\Theta(0)}{d\kappa} = 0, \tag{19}$$

where  $\Re$  is the Reynolds number,  $P_r$  is the Prandtl number, and  $E_c$  is the Eckert number.

The Reynolds number can be classified as:

$$\Re = \frac{u_c \rho_f \gamma}{\mu_f} = \frac{U_{max} r \rho_f \gamma}{\mu_f} \times \begin{pmatrix} \text{divergent - channel: } \gamma > 0, u_c > 0 \\ \text{convergent - channel: } \gamma < 0, u_c < 0 \end{pmatrix}. \tag{20}$$

$$P_r = \frac{\mu_f (C_p)_f}{K_f}. \tag{21}$$

$$E_c = \frac{u_c^2}{T_w (C_p)_f}. \tag{22}$$

The skin friction coefficient ( $\tilde{C}_f$ ) and shear stress ( $\sigma_w$ ) are defined:

$$\tilde{C}_f = \frac{\sigma_w}{\rho_f U_{max}^2} \text{ and } \sigma_w = \mu_{n.f} \left( \frac{1}{r} \frac{\partial u(r, \theta)}{\partial \theta} \right), \tag{23}$$

substituting Eq. (10) into Eq. (23), the skin friction coefficient is:

$$\tilde{C}_f = \frac{1}{\tilde{R}_e(1-\varphi)^{2.5}} \frac{d\tilde{h}(1)}{d\kappa}. \tag{24}$$

The local Nusselt number  $\tilde{N}_u$  (heat transfer rate) is:

$$\tilde{N}_u = \frac{rg_w|_{\theta=\gamma}}{K_f T_w}, \quad g_w = -K_{n.f} \nabla T, \tag{25}$$

the equation above in view of Eq (11) becomes:

$$\tilde{N}_u = -\frac{1}{\gamma} \frac{K_{n.f}}{K_f} \frac{d\theta(1)}{d\kappa}. \tag{26}$$

Physically, these boundary constraints imply that the maximum velocity values are seen at the center line ( $\kappa = 0$ ) . If we consider the velocity profile to be completely developed, then the rate of velocity is zero at  $\kappa = 0$ . The no-slip requirement is also used in fluid dynamics. The equation of the fluid states that the fluid will have zero pressure at a solid barrier related to the boundary velocity at all fluid–solid interfaces. The fluid velocity can observe that the solid boundary border is equal to the solid boundaries.

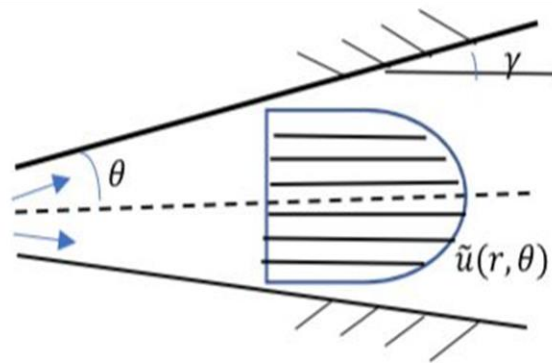


Figure 1: Diagram of the problem [8].

### 3. Implementation of Perturbation Iteration Scheme for Solving heat transfer on Jeffery-Hamel Nanofluid Flow:

The stages of the method of the PIS (1,1) [23] apply to the nonlinear differential equations to obtain the approximate analytical solutions. The following is an illustration of the auxiliary perturbation parameter  $\delta$  which can be given as follows:

$$Q_1(\tilde{h}(\kappa), \frac{\partial \tilde{h}(\kappa)}{\partial \kappa}, \frac{\partial^3 \tilde{h}(\kappa)}{\partial \kappa^3}, \delta) = \frac{d^3 \tilde{h}(\kappa)}{d\kappa^3} + 2\delta\gamma\mathfrak{R}[(1-\varphi) + \varphi \frac{\rho_s}{\rho_f}] (1-\varphi)^{2.5} \tilde{h}(\kappa) \frac{d\tilde{h}(\kappa)}{d\kappa} + 4\delta\gamma^2 \frac{d\tilde{h}(\kappa)}{d\kappa} = 0, \tag{27}$$

$$Q_2(\tilde{h}(\kappa), \frac{\partial \tilde{h}(\kappa)}{\partial \kappa}, \Theta(\kappa), \frac{\partial^2 \Theta(\kappa)}{\partial \kappa^2}, \delta) = \frac{1}{[(1-\varphi) + \varphi \frac{(\rho C \rho)_s}{(\rho C \rho)_f}]} \left[ \frac{K_{n.f}}{K_f} \frac{d^2 \Theta(\kappa)}{d\kappa^2} + \frac{P_r E_c}{(1-\varphi)^{2.5}} \delta (4\gamma^2 (\tilde{h}(\kappa))^2 + (\frac{d\tilde{h}(\kappa)}{d\kappa})^2) \right] = 0. \tag{28}$$

The following are perturbation expansions that only include one correction term:

$$\tilde{h}_{n+1} = \tilde{h}_n + \delta(\tilde{h}_c)_n, \tag{29}$$

$$\Theta_{n+1} = \Theta_n + \delta(\Theta_c)_n, \tag{30}$$

substituting Eq. (29), and (30) in Eqs. (27), and (28), respectively, then expanding in Taylor series with first -order derivative with term of  $(\delta = 0)$  to get:

$$Q_1((\hbar(\kappa))_n, (\frac{d\hbar(\kappa)}{d\kappa})_n, (\frac{d^3\hbar(\kappa)}{d\kappa^3})_n, 0) + \delta[Q_{1\hbar_n}((\hbar(\kappa))_c)_n + Q_1(\frac{d\hbar(\kappa)}{d\kappa})_n ((\frac{d\hbar(\kappa)}{d\kappa})_c)_n + Q_1(\frac{d^3\hbar(\kappa)}{d\kappa^3})_n ((\frac{d^3\hbar(\kappa)}{d\kappa^3})_c)_n + Q_{1\delta}] = 0, \tag{31}$$

$$Q_2((\hbar(\kappa))_n, (\frac{d\hbar(\kappa)}{d\kappa})_n, (\frac{d^2\Theta(\kappa)}{d\kappa^2})_n, 0) + \delta[Q_{2(\hbar(\kappa))_n}((\hbar(\kappa))_c)_n + Q_2(\frac{d\hbar(\kappa)}{d\kappa})_n ((\frac{d\hbar(\kappa)}{d\kappa})_c)_n + Q_2(\frac{d^2\Theta(\kappa)}{d\kappa^2})_n ((\frac{d^2\Theta(\kappa)}{d\kappa^2})_c)_n + Q_{2\delta}] = 0, \tag{32}$$

from Eqs. (27), and (28), the following derivatives:

$$Q_{1(\hbar(\kappa))_n} = 2\delta\gamma\Re[(1 - \varphi) + \varphi\frac{\rho_s}{\rho_f}](1 - \varphi)^{2.5}(\frac{d\hbar(\kappa)}{d\kappa})_n, \\ Q_{1(\frac{d\hbar(\kappa)}{d\kappa})_n} = 2\delta\gamma\Re[(1 - \varphi) + \varphi\frac{\rho_s}{\rho_f}](1 - \varphi)^{2.5}(\hbar(\kappa))_n + 4\delta\gamma^2, \\ Q_{1(\frac{d^3\hbar(\kappa)}{d\kappa^3})_n} = 1, \\ Q_{1\delta} = 2\gamma\Re[(1 - \varphi) + \varphi\frac{\rho_s}{\rho_f}](1 - \varphi)^{2.5}(\hbar(\kappa))_n(\frac{d\hbar(\kappa)}{d\kappa})_n + 4\gamma^2(\frac{d\hbar(\kappa)}{d\kappa})_n, \tag{33}$$

$$Q_{2\delta} = \frac{1}{[(1-\varphi)+\varphi\frac{(\rho C\rho)_s}{(\rho C\rho)_f}]} \left[ \frac{PrEc}{(1-\varphi)^{2.5}} (4\gamma^2((\hbar(\kappa))_n)^2 + ((\frac{d\hbar(\kappa)}{d\kappa})_n)^2) \right] = 0, \\ Q_{2(\hbar(\kappa))_n} = \frac{1}{[(1-\varphi)+\varphi\frac{(\rho C\rho)_s}{(\rho C\rho)_f}]} \left[ \frac{PrEc}{(1-\varphi)^{2.5}} (8\delta\gamma^2(\hbar(\kappa))_n) \right], \\ Q_{2(\frac{d\hbar(\kappa)}{d\kappa})_n} = \frac{1}{[(1-\varphi)+\varphi\frac{(\rho C\rho)_s}{(\rho C\rho)_f}]} \left[ \frac{PrEc}{(1-\varphi)^{2.5}} (2\delta(\frac{d\hbar(\kappa)}{d\kappa})_n) \right], \\ Q_{2(\frac{d^2\Theta(\kappa)}{d\kappa^2})_n} = \frac{K_{n,f}/K_f}{[(1-\varphi)+\varphi\frac{(\rho C\rho)_s}{(\rho C\rho)_f}]} . \tag{34}$$

The following nonlinear ordinary differential equations are obtained by computing all derivatives at  $(\delta = 0)$  and inserting the results into Eqs. (31) and (32),

$$((\frac{d^3\hbar(\kappa)}{d\kappa^3})_c)_n = \frac{-1}{\delta} (\frac{d^3\hbar(\kappa)}{d\kappa^3})_n - 2\gamma\Re[(1 - \varphi) + \varphi\frac{\rho_s}{\rho_f}] (1 - \varphi)^{2.5} (\hbar(\kappa))_n (\frac{d\hbar(\kappa)}{d\kappa})_n + 4\gamma^2 (\frac{d\hbar(\kappa)}{d\kappa})_n. \tag{35}$$

$$((\frac{d^2\Theta(\kappa)}{d\kappa^2})_c)_n = \frac{1}{[(1-\varphi)+\varphi\frac{(\rho C\rho)_s}{(\rho C\rho)_f}]} \left[ \frac{-1}{\delta} \frac{K_{n,f}}{K_f} (\frac{d^2\Theta(\kappa)}{d\kappa^2})_n - \frac{PrEc}{(1-\varphi)^{2.5}} (4\gamma^2((\hbar(\kappa))_n)^2 + ((\frac{d\hbar(\kappa)}{d\kappa})_n)^2) \right], \tag{36}$$

Assume that the initial conditions,

$$\hbar_o(\kappa) = \tau_o + \tau_1\kappa + \frac{\tau_2}{2}\kappa^2, \tag{37}$$

$$\Theta_o(\kappa) = \ell_o + \ell_1\kappa, \tag{38}$$

where:

$$\hbar(0) = \tau_o, \quad \frac{d\hbar(0)}{d\kappa} = \tau_1, \quad \frac{d^2\hbar(\kappa)}{d\kappa^2} = \tau_2, \\ \Theta(0) = \ell_o, \quad \frac{d\Theta(\kappa)}{d\kappa} = \ell_1. \tag{39}$$

From the boundary conditions of Eq. (19):

$$\hbar_o = 1 + \frac{\tau_2}{2}\kappa^2, \tag{40}$$

$$\Theta_o = \ell_o. \tag{41}$$

The prerequisite condition for solving the problem using  $\tau_2$  and  $\ell_o$  is unknown. The analytical approximate solutions of Eqs. (15) and (18), at  $\kappa = 1$  may be used to derive the

values of  $\tau_2$  and  $\ell_0$ . The analytical approximate solutions to the following equations are obtained by creating the iteration scheme:

$$\hbar_1 = 1 + \frac{\tau_2}{2} \kappa^2 + \left(\frac{-1}{12} \gamma [(1 - \varphi) + \varphi \frac{\rho_s}{\rho_f}] (1 - \varphi)^{2.5} \Re \tau_2 - \frac{1}{24} 4\gamma^2 \tau_2\right) \kappa^4 - \frac{1}{120} \gamma \Re \tau_2^2 \kappa^6. \quad (42)$$

$$\Theta_1 = \ell_0 - \frac{2\gamma^2}{(1-\varphi+P\varphi)(1-\varphi)^{2.5}} P_r E_c \kappa^2 - \frac{1}{12} \frac{P_r E_c (4\gamma^2 \tau_0 + \tau_0^2)}{(1-\varphi+P\varphi)(1-\varphi)^{2.5}} \kappa^4 - \frac{1}{30} \frac{\gamma^2 P_r E_c}{(1-\varphi+P\varphi)(1-\varphi)^{2.5}} \tau_0^2 \kappa^6. \quad (43)$$

$$\begin{aligned} \hbar_2 = & 1 + \frac{\tau_2}{2} \kappa^2 + \left(\frac{-1}{12} \gamma [(1 - \varphi) + \varphi \frac{\rho_s}{\rho_f}] (1 - \varphi)^{2.5} \Re \tau_2 \right. \\ & - \frac{1}{6} 4\gamma^2 \tau_2\right) \kappa^4 + \left(\frac{-1}{180} \gamma^3 [(1 - \varphi) + \varphi \frac{\rho_s}{\rho_f}] (1 - \varphi)^{2.5} \Re \tau_2 + \right. \\ & \left. \frac{1}{180} \gamma^2 [(1 - \varphi) + \varphi \frac{\rho_s}{\rho_f}]^2 (1 - \varphi)^5 \Re^2 \tau_2 + \frac{1}{45} \gamma^3 [(1 - \varphi) + \varphi \frac{\rho_s}{\rho_f}] \right. \\ & \left. (1 - \varphi)^{2.5} \Re \tau_2 - \frac{1}{120} \gamma [(1 - \varphi) + \varphi \frac{\rho_s}{\rho_f}] (1 - \varphi)^{2.5} \Re \tau_2^2 + \right. \\ & \left. \frac{1}{45} \gamma^4 \tau_2\right) \kappa^6 + \left(\frac{-1}{1120} \gamma^3 \Re \tau_2^2 \tau + \frac{1}{560} [(1 - \varphi) + \varphi \frac{\rho_s}{\rho_f}]^2 (1 - \varphi)^5 \gamma^3 \Re^2 \tau_2^2 \right. \\ & + \frac{1}{280} \gamma^3 [(1 - \varphi) + \varphi \frac{\rho_s}{\rho_f}] (1 - \varphi)^{2.5} \Re \tau_2^2\right) \kappa^8 + \left(\frac{1}{12960} \gamma^4 [(1 - \varphi) + \varphi \frac{\rho_s}{\rho_f}]^2 \right. \\ & \left. (1 - \varphi)^5 \Re^2 \tau_2^2 - \frac{1}{51840} \gamma^3 [(1 - \varphi) + \varphi \frac{\rho_s}{\rho_f}] (1 - \varphi)^{2.5} \Re \tau_2^2 + \frac{1}{6480} \gamma^5 [(1 - \varphi) \right. \\ & \left. + \varphi \frac{\rho_s}{\rho_f}] (1 - \varphi)^{2.5} \Re \tau_2^2 - \frac{1}{3240} \gamma^5 [(1 - \varphi) + \varphi \frac{\rho_s}{\rho_f}] (1 - \varphi)^{2.5} \Re \tau_2^2 + \frac{1}{10800} \gamma^2 \right. \\ & \left. [(1 - \varphi) + \varphi \frac{\rho_s}{\rho_f}]^2 (1 - \varphi)^5 \Re^2 \tau_2^3 - \frac{1}{12960} \gamma^3 [(1 - \varphi) + \varphi \frac{\rho_s}{\rho_f}]^3 (1 - \varphi)^{7.5} \Re^3 \tau_2^2 \right. \\ & \left. - \frac{1}{3240} \gamma^4 [(1 - \varphi) + \varphi \frac{\rho_s}{\rho_f}]^2 (1 - \varphi)^5 \Re^2 \tau_2^2\right) \kappa^{10} + \left(\frac{1}{190080} \gamma^4 [(1 - \varphi) + \varphi \frac{\rho_s}{\rho_f}]^2 \right. \\ & \left. (1 - \varphi)^5 \Re^2 \tau_2^3 - \frac{1}{95040} \gamma^3 [(1 - \varphi) + \varphi \frac{\rho_s}{\rho_f}]^3 (1 - \varphi)^{7.5} \Re^3 \tau_2^3 \right. \\ & \left. [(1 - \varphi) + \varphi \frac{\rho_s}{\rho_f}]^2 (1 - \varphi)^5 \Re^2 \tau_2^3\right) \kappa^{12} - \frac{1}{2620800} \gamma^3 [(1 - \varphi) + \varphi \frac{\rho_s}{\rho_f}]^3 \\ & \left. (1 - \varphi)^{7.5} \Re^3 \tau_2^4\right) \kappa^{14}. \end{aligned} \quad (44)$$

$$\begin{aligned} \Theta_2 = & \ell_0 - \frac{4\gamma^2 P_r E_c}{(1-\varphi+P\varphi)(1-\varphi)^{2.5}} \kappa^2 - \frac{1}{3} \frac{P_r E_c (4\gamma^2 \tau_0 + \tau_0^2) K}{(1-\varphi+P\varphi)^2 (1-\varphi)^{2.5}} \kappa^3 \\ & - \frac{1}{6} \frac{P_r E_c (4\gamma^2 \tau_0 + \tau_0^2)}{(1-\varphi+P\varphi)(1-\varphi)^{2.5}} \kappa^4 - \frac{1}{5} \frac{\gamma^2 P_r E_c K}{(1-\varphi+P\varphi)^2 (1-\varphi)^{2.5}} \tau_0 \kappa^5 + \left[\frac{1}{45} \frac{\gamma^2 P_r E_c \Re}{(1-\varphi+P\varphi)^2} \tau_0 \right. \\ & \left. - \frac{2}{45} \frac{\gamma^4 P_r E_c}{(1-\varphi+P\varphi)(1-\varphi)^{2.5}} \tau_0 + \frac{1}{15} \frac{\gamma^2 P_r E_c}{(1-\varphi+P\varphi)(1-\varphi)^{2.5}} \tau_0^2 + \frac{1}{45} \gamma P_r E_c \tau_0^2 - \frac{2}{45} \frac{\gamma^2 P_r E_c}{(1-\varphi+P\varphi)(1-\varphi)^{2.5}} \tau_0^2\right] \kappa^6 \\ & + \left[\frac{1428}{1200000} \gamma^2 P_r E_c \Re \tau_0^2 + \frac{1428}{240000} \gamma^2 P_r E_c \tau_0^2 - \frac{1428}{120000} \frac{\gamma^4 P_r E_c}{(1-\varphi+P\varphi)(1-\varphi)^{2.5}} \tau_0^2 - \frac{357}{200000} \gamma P_r E_c \Re \tau_0^3 \right. \\ & \left. + \frac{357}{20000} \frac{P_r E_c}{(1-\varphi+P\varphi)(1-\varphi)^{2.5}} \left(-\frac{1}{3} (1 - \varphi + P\varphi) (1 - \varphi)^{2.5} \gamma \Re \tau_0 - \frac{2}{3} \gamma^2 \tau_0\right)^2\right] \kappa^8 + \\ & \left[\frac{1}{2700} \gamma^3 P_r E_c \Re \tau_0^3 + \frac{2}{45} \frac{\gamma^2 P_r E_c}{(1-\varphi+P\varphi)(1-\varphi)^{2.5}} \left(-\frac{1}{12} (1 - \varphi + P\varphi) (1 - \varphi)^{2.5} \gamma \Re \tau_0 - \frac{1}{6} \lambda^2 \tau_0\right)^2 \right. \\ & \left. - \frac{1}{2700} (1 - \varphi + P\varphi) (1 - \varphi)^{2.5} \gamma^2 P_r E_c \Re^2 \tau_0^3 - \frac{2}{2700} \gamma^4 P_r E_c \tau_0^3\right] \kappa^{10} + \left[\frac{1}{142560} \right. \\ & \left. (1 - \varphi + P\varphi) (1 - \varphi)^{2.5} \gamma^4 P_r E_c \Re^2 \tau_0^3 - \frac{1}{71280} \gamma^5 P_r E_c \tau_0^3 + \frac{1}{52800} (1 - \varphi + P\varphi) \right. \\ & \left. (1 - \varphi)^{2.5} \gamma^2 P_r E_c \Re^2 \tau_0^4\right] \kappa^{12} - [0.001526251526 \frac{(1-\varphi+P\varphi)}{(1-\varphi)^{2.5}} \gamma^4 P_r E_c \Re^2 \tau_0^4] \kappa^{14}. \end{aligned} \quad (45)$$

#### 4. Results and discussions:

The PIS is used to get an approximate analytic solution to the nonlinear differential governing equations (15) and (18) with the required boundary conditions in Eq. (19). The fourth-order Runge-Kutta Scheme is also used to solve the problem numerically. Table 1 shows the thermo-physical properties of four distinct kinds of nanoparticles. Discussions of various flow parameters, namely volume fraction, Reynolds number, open angle, Prandtl number, and Eckert number according to the velocity profile  $\hbar(\kappa)$  and temperature distribution  $\Theta(\kappa)$  are

included. The convergence of values  $\tau_2$  is clearly shown in Tables 2 and 3. In Table 4, the PIS findings are presented and compared to DTM [7], HPM [8], OHAM [9], SHAM [10], and HAM [11]. The results are totally compatible in this table. Tables 5-12 present the nanomaterials and the influence of the velocity and temperature profiles of the channel convergence and divergence, which shows the result that the solutions are compatible compared to Range-Kutta of the fourth order. Table 13 shows the numerical values of the skin friction coefficient for different values of Reynolds number and solid volume fraction for the three types of nanoparticles at the convergent and divergent channels, which results in incongruity in the values and contrast with other methods as we have seen. Tables 14-16 show variation in the Nusselt number with varying open angles, Prandtl number and Eckert number in both converge and diverge channels, when varying the Prandtl number and the Eckert number, we found that the values are growing in both converge and divergent channel. However, if we vary the angle, there is a rising in the convergent channel and in the divergent channel, the values are decreasing. Finally, in Table 17, we discussed the effect of the nanoparticle on the critical Reynolds numbers in the divergent channel, this precision establishes the validity of the problem and demonstrates a high level of the engineering precision. Illustrating the impacts of key factors leads to determine how these variables that affect the fluid.

**Table 1:** Thermos physical properties of nanofluids and nanoparticles [22]

Material	$\rho(\text{kg/m}^3)$	$C_p(\text{j/kgk})$	$k(\text{W/mk})$
Clear water	997.1	4179	0.613
Ag	10500	235	429
Cu	8933	385	400
$\text{Al}_2\text{O}_3$	3970	765	40
$\text{TiO}_2$	4250	686.2	8.9538

**Table 2:** The convergence values for the nanoparticles materials when  $\phi = 0.02$

Order	$\Re = 10$			
	$\gamma = 5^\circ$			
	$\tau_2$			
	Ag	Cu	$\text{TiO}_2$	$\text{Al}_2\text{O}_3$
Order <sup>1</sup>	-2.2969835	-2.2885436	-2.2635654	-2.2620835
Order <sup>2</sup>	-2.2862095	-2.2783414	-2.2549735	-2.2535832
Order <sup>3</sup>	-2.2864504	-2.2785635	-2.2551454	-2.2537525
Order <sup>4</sup>	-2.2864471	-2.2785606	-2.2551433	-2.2537504
Order <sup>5</sup>	-2.2864471	-2.2785606	-2.2551434	-2.2537504

**Table 3:** The convergence values for the nanoparticles materials when  $\phi = 0.02$

Order	$\Re=10$			
	$\gamma = -5^\circ$			
	$\tau_2$			
	Ag	Cu	$\text{TiO}_2$	$\text{Al}_2\text{O}_3$
Order <sup>1</sup>	-1.7652708	-1.7710062	-1.7883277	-1.7893721
Order <sup>2</sup>	-1.7575697	-1.7636892	-1.7821083	-1.7832159
Order <sup>3</sup>	-1.7574089	-1.7635406	-1.7819925	-1.7831019
Order <sup>4</sup>	-1.7574067	-1.7635386	-1.7819911	-1.7831005
Order <sup>5</sup>	-1.7574067	-1.7635386	-1.7819911	-1.7831005

**Table 4:** The results of PIS for  $\hbar(\kappa)$  and compare with numerical methods when  $\Re=50$  and  $\gamma = 5^\circ$

$\kappa$	PIS	HPM[8]	OHAM[9]	SHAM[10]	DTM[7]
0.00	1.0000000000	1.0000000000	1.000000000	1.000000	1.000000
0.10	0.9824360735	0.9824314771	0.98251808	0.982431	0.982431
0.20	0.9312441309	0.9312268428	0.93156588	0.931226	0.931226
0.30	0.8506474490	0.8506123257	0.85138150	0.850611	0.850611
0.40	0.7468472398	0.7467931374	0.74826039	0.746791	0.746791
0.50	0.6270205474	0.6269505503	0.62953865	0.626848	0.626948
0.60	0.4983150189	0.4982362037	0.50242894	0.498234	0.498234
0.70	0.3670440934	0.3669671316	0.37293383	0.366966	0.366966
0.80	0.2381851869	0.2381237540	0.24508197	0.238124	0.238124
0.90	0.1151819641	0.1151516618	0.12071560	0.115152	0.115152
1.00	0.0000000000	0.0000000000	0.00000010	0.000000	0.000000

**Table 5:** The results of PIS for  $\hbar(\kappa)$  and  $\Theta(\kappa)$  of Cu when  $\gamma = 1^\circ, \varphi=0.04$

$\kappa$	$\Re = 1$		$\Re = 1$	
	$\hbar(\kappa)$	RK4S	$\Theta(\kappa)$	RK4S
0.00	1.0000000000	1.0000000000	1.000374384	1.000374384
0.20	0.9598906079	0.9598906105	1.000373949	1.000373858
0.40	0.8396283565	0.8396283491	1.000367660	1.000366257
0.60	0.6393949783	0.6393948180	1.000340552	1.000333545
0.80	0.3594398924	0.3594391035	1.000267690	1.000245772

**Table 6:** The results of PIS for  $\hbar(\kappa)$  and  $\Theta(\kappa)$  of  $TiO_2$  when  $\gamma = 1^\circ, \varphi=0.04$

$\kappa$	$\Re = 1$		$\Re = 1$	
	$\hbar(\kappa)$	RK4S	$\Theta(\kappa)$	RK4S
0.00	1.0000000000	1.000000000	1.000375989	1.000375989
0.20	0.9599056675	0.9599056696	1.000375540	1.000375452
0.40	0.8396794570	0.8396794528	1.000369042	1.000367678
0.60	0.6394779859	0.6394778697	1.000341035	1.000334213
0.80	0.3595164696	0.3595158875	1.000265759	1.000244396

**Table 7:** The results of PIS for  $\hbar(\kappa)$  and  $\Theta(\kappa)$  of  $Al_2O_3$  when  $\gamma = 1^\circ, \varphi=0.04$

$\kappa$	$\Re = 1$		$\Re = 1$	
	$\hbar(\kappa)$	RK4S	$\Theta(\kappa)$	RK4S
0.00	1.0000000000	1.000000000	1.000375531	1.000375531
0.20	0.9599065675	0.9599065698	1.000375094	1.000375004
0.40	0.8396825114	0.8396825075	1.000368743	1.000367390
0.60	0.6394829476	0.6394828339	1.000341376	1.000334612
0.80	0.3595210469	0.3595204763	1.000267818	1.000246637

**Table 8:** The results of PIS for  $\hbar(\kappa)$  and  $\Theta(\kappa)$  of Ag when  $\gamma = 1^\circ, \varphi=0.04$

$\kappa$	$\Re = 1$		$\Re = 1$	
	$\hbar(\kappa)$	RK4S	$\Theta(\kappa)$	RK4S
0.00	1.0000000000	1.0000000000	1.000378034	1.000386668
0.20	0.9598855669	0.9599192950	1.000377595	1.000386161
0.40	0.8396112513	0.8397256918	1.000371244	1.000378823
0.60	0.6393671939	0.6395530144	1.000343875	1.000347230
0.80	0.3594142621	0.3595853457	1.000270305	1.000262418

**Table 9:** The results of PIS for  $\hbar(\kappa)$  and  $\Theta(\kappa)$  of Cu when  $\gamma = -1^\circ, \varphi=0.04$

$\kappa$	$\Re = 1$		$\Re = 1$	
	$\hbar(\kappa)$	RK4S	$\Theta(\kappa)$	RK4S
0.00	1.0000000000	1.0000000000	1.000370267	1.000370267
0.20	0.9601011710	0.9601011681	1.000369837	1.000369748
0.40	0.8403429937	0.8403429665	1.000363616	1.000362216
0.60	0.6405562611	0.6405560746	1.000336806	1.000329726
0.80	0.3605118416	0.3605110826	1.000264745	1.000242260

**Table 10 :** The results of PIS for  $\hbar(\kappa)$  and  $\Theta(\kappa)$  of  $Al_2O_3$  when  $\gamma = -1^\circ, \varphi=0.04$

$\kappa$	$\Re = 1$		$\Re = 1$	
	$\hbar(\kappa)$	RK4S	$\Theta(\kappa)$	RK4S
0.00	1.0000000000	1.0000000000	1.000372021	1.000372021
0.20	0.9600720270	0.9600853290	1.000371586	1.000371498
0.40	0.8402359899	0.8402892035	1.000365291	1.000363942
0.60	0.6403490232	0.6404687182	1.000338162	1.000331354
0.80	0.3602179793	0.3604305663	1.000265243	1.000243641

**Table 11:** The results of PIS for  $\hbar(\kappa)$  and  $\Theta(\kappa)$  of  $TiO_2$  when  $\gamma = -1^\circ, \varphi=0.04$

$\kappa$	$\Re = 1$		$\Re = 1$	
	$\hbar(\kappa)$	RK4S	$\Theta(\kappa)$	RK4S
0.00	1.0000000000	1.0000000000	1.000372440	1.000372440
0.20	0.9600862253	0.9600862229	1.000371995	1.000371908
0.40	0.8402922588	0.8402922376	1.000365558	1.000364195
0.60	0.6404737867	0.6404736481	1.000337815	1.000330925
0.80	0.3604356670	0.3604351106	1.000263250	1.000241379

**Table 12:** The results of PIS for  $\hbar(\kappa)$  and  $\Theta(\kappa)$  of Ag when  $\gamma = -1^\circ, \varphi=0.04$

$\kappa$	$\Re = 1$		$\Re = 1$	
	$\hbar(\kappa)$	RK4S	$\Theta(\kappa)$	RK4S
0.00	1.0000000000	1.0000000000	1.000373679	1.000383565
0.20	0.9601061701	0.9600726854	1.000373245	1.000383061
0.40	0.8403599641	0.8402462881	1.000366967	1.000375772
0.60	0.6405838490	0.6403989861	1.000339912	1.000344335
0.80	0.3605373237	0.3603662792	1.000267190	1.000259738

**Table 13 :** Numerical values of coefficient skin friction for different values of  $\Re$  and solid fraction volume for three types of nanoparticle and  $\gamma = 5^\circ$ .

$\Re$	$\varphi = 0$		$\varphi = 0.1$					
	PIS	Reference [10]	PIS			Reference [10]		
			Cu	$TiO_2$	$Al_2O_3$	Cu	$TiO_2$	$Al_2O_3$
10	-0.181958	-0.181931	0.135745	0.1401575	0.1404253	0.228015	0.236316	0.236812
30	-0.048962	-0.048809	-	-	-	-	-	-
50	-0.022567	-0.022186	0.035031	0.0388974	0.0391311	0.054721	0.063075	0.063575
			0.014416	0.0189198	0.0191634	0.020245	0.028433	0.028929

**Table 14:** Variation in  $\tilde{N}_u$  with varying  $P_r$  for Cu

$\Re = 25, E_c = 0.01, \varphi = 0.1$		
$-\gamma\tilde{N}_u = \frac{K_{n,f}}{K_f} \frac{d\theta(1)}{d\kappa}$		
$P_r$	$\gamma = 5^\circ$	$\gamma = -5^\circ$
0.5	0.0934957060	0.006617359722
1.0	0.1869914120	0.013234719500
1.5	0.2804871179	0.019852079230
2.0	0.3739828239	0.026469438950
2.5	0.4674785302	0.033086798680

**Table 15 :** Variation in  $\tilde{N}_u$  with varying  $\gamma$  for Cu.

$\Re = 25, P_r = 0.5, \varphi = 0.1, E_c = 0.01$			
$-\gamma\tilde{N}_u = \frac{K_{n,f}}{K_f} \frac{d\theta(1)}{d\kappa}$			
$\gamma$		$\gamma$	
$0^\circ$	0.03833679214	$0^\circ$	0.03833679214
$2^\circ$	0.02034918052	$-2^\circ$	0.05263417385
$4^\circ$	0.01046665925	$-4^\circ$	0.07783864594
$6^\circ$	0.00335442152	$-6^\circ$	0.11156570240

**Table 16:** Variation in  $\tilde{N}_u$  with varying  $E_c$  for Cu

$\Re = 25, P_r = 0.5, \varphi = 0.1$		
$-\gamma\tilde{N}_u = \frac{K_{n,f}}{K_f} \frac{d\theta(1)}{d\kappa}$		
$E_c$	$\gamma = 5^\circ$	$\gamma = -5^\circ$
0.1	0.9349570422	0.0066173599
0.2	1.8699140860	0.1323471987
0.3	2.8048711300	0.1985207982
0.4	3.7398281700	0.2646943973
0.5	4.6747852130	0.3308679970

**Table 17:** The effect of nanoparticles on critical Reynolds numbers in the divergent channel when  $\gamma = 5^\circ$

$\Re$	$\hat{h}(1)$				
	$\varphi = 0$	$\varphi = 0.1$			
		Ag	Cu	Al <sub>2</sub> O <sub>3</sub>	TiO <sub>2</sub>
50	-0.024902	-0.135720	-0.144161	-0.019163	-0.189198
60	-0.018192	-0.007012	-0.008602	-0.012684	-0.012433
80	-0.009106	-0.002543	-0.002776	-0.006684	-0.006445
100	-0.004075	-0.003458	-0.001749	-0.003156	-0.002938

Figures 2-5 evidence the effect of the different values of the solid volume fraction. It is clear in both profile velocity and normalized temperature for all four materials Water – Cu , Water – Ag, Water – Al<sub>2</sub>O<sub>3</sub>, and Water – TiO<sub>2</sub> . These figures prove that the increase in the normalized temperature at all materials with  $\Re = 50, \gamma = 5^\circ$  and the normalized velocity decreases in (Cu, Ag) and increases in (Al<sub>2</sub>O<sub>3</sub>, TiO<sub>2</sub>). Figures 6 and 7 show a comparison of the four materials Ag, Cu , TiO<sub>2</sub> and Al<sub>2</sub>O<sub>3</sub> with  $\Re = 50, \gamma = \mp 5^\circ, \varphi = 0.2$ . These figures indicate that there are decreasing in the velocity profile and increment normalized temperature in converge channel, whereas, in the divergent channel increment in velocity profile and

temperature profile, they are decreasing. Also, Figures 8 and 9 display the behavior of the velocity profile and normalized temperature for varying open angle and Reynolds number in the divergent channel, which clearly shows the decrease in the velocity profile, while the profile temperature is increasing. Figures 10 and 11 illustrate the influences of the different Eckert numbers. The Prandtl number can be obviously realized that the result is similar to the open angle and Reynolds number, however, there is difference in the behaviors of the curve's velocity that have no effect for several of the Eckert number and the Prandtl number.

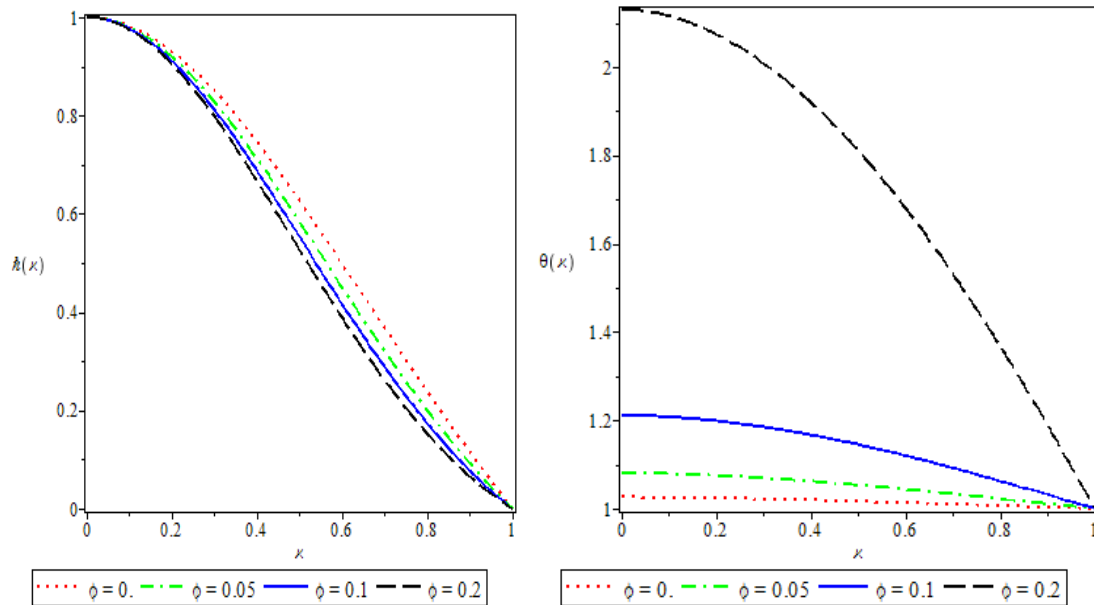


**Figure 2:** Normalized velocity profile and Normalized temperature with different types of solid volume fraction for water-Ag nanofluid when  $\Re = 50$  ,  $\gamma = 5^\circ$ .

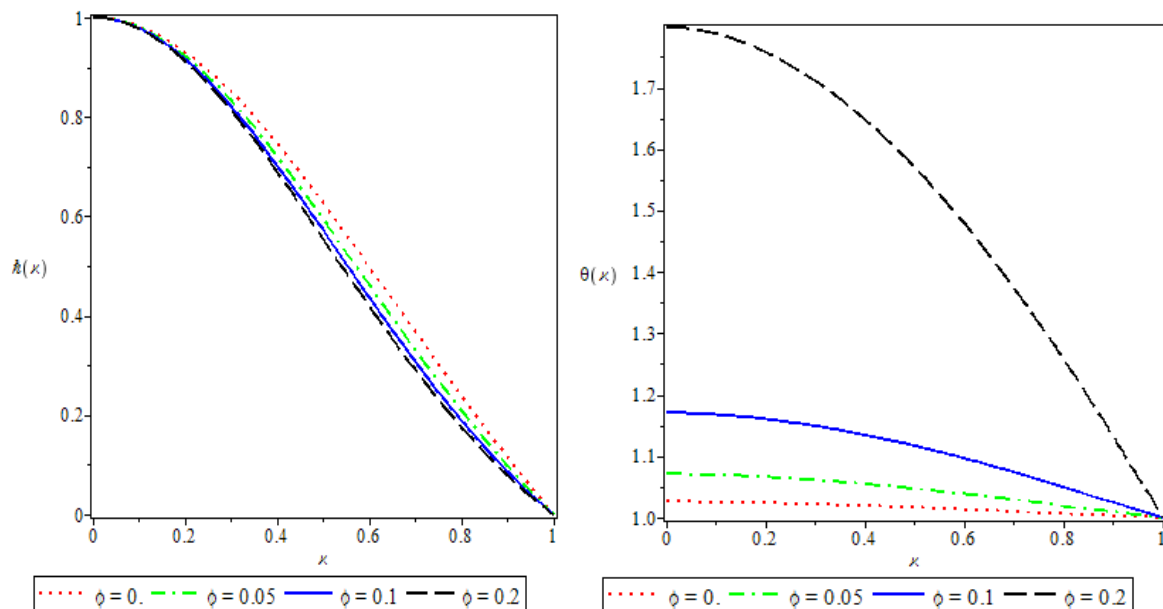


**Figure 3:** Normalized velocity profile and Normalized temperature with different types of solid volume fraction for water-Cu nanofluid when  $\Re = 50$  ,  $\gamma = 5^\circ$ .

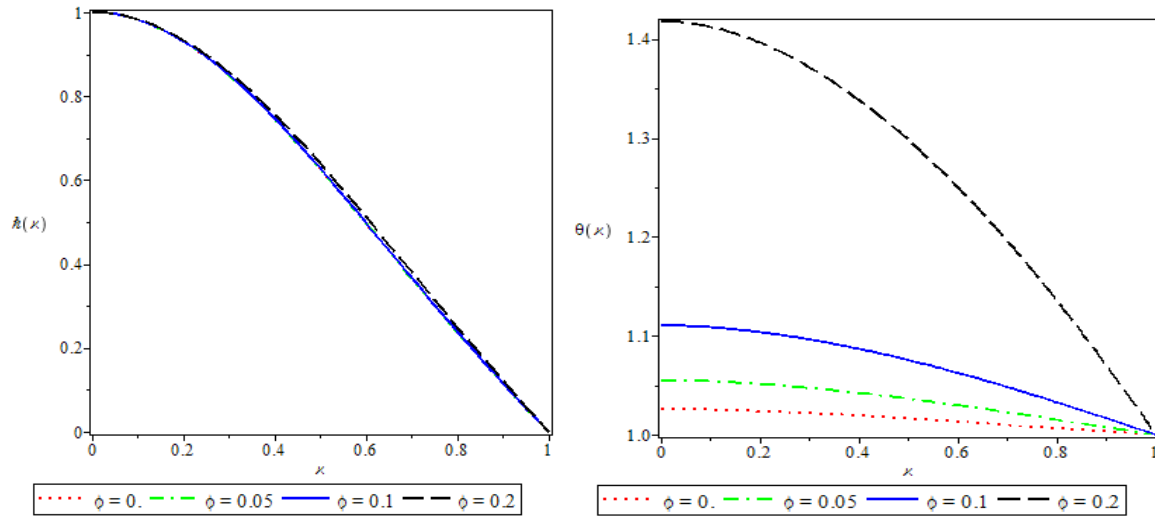


**Figure 4:** Normalized velocity profile and Normalized temperature with different types of solid volume fraction for water- $Al_2O_3$  nanofluid when  $\Re = 50$  ,  $\gamma = 5^\circ$ .

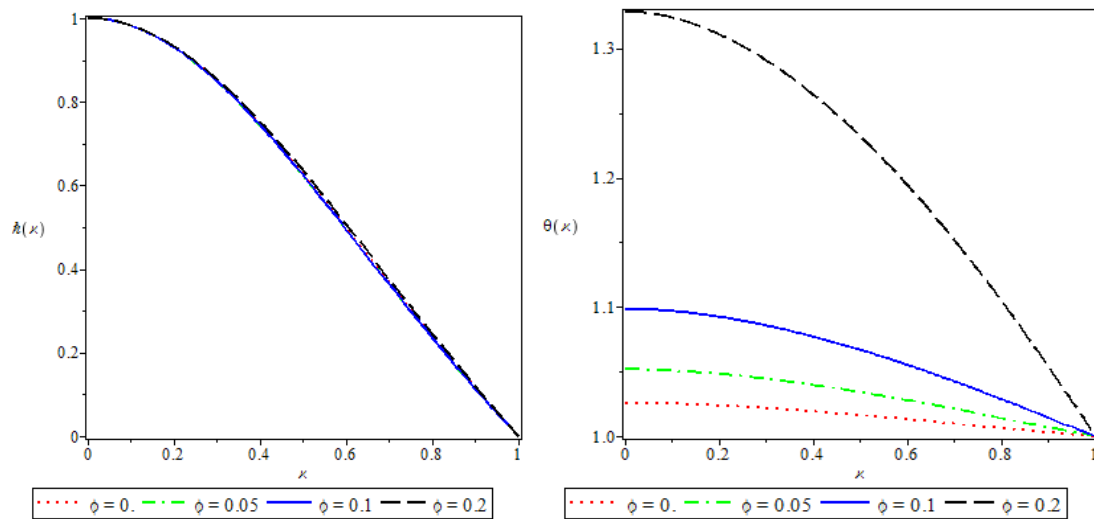


**Figure 5:** Normalized velocity profile and Normalized temperature with different types of solid volume fraction for water- $TiO_2$  nanofluid when  $\Re = 50$  ,  $\gamma = 5^\circ$ .Q

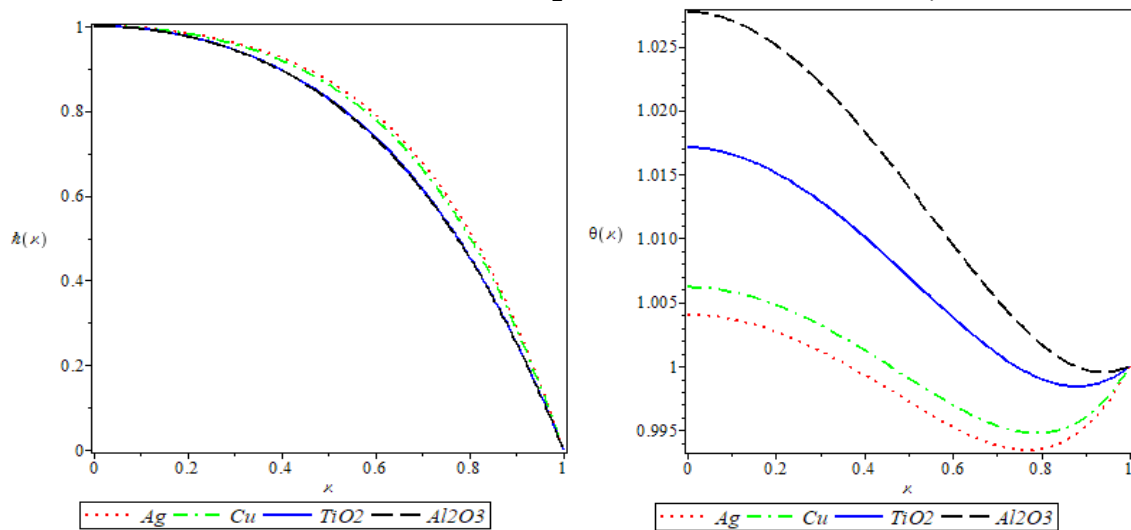


**Figure 6:** Normalized velocity profile and Normalized temperature for three types nanoparticles nanofluid when  $\Re = 50$  ,  $\gamma = -5^\circ$  ,  $\phi = 0.2$  .

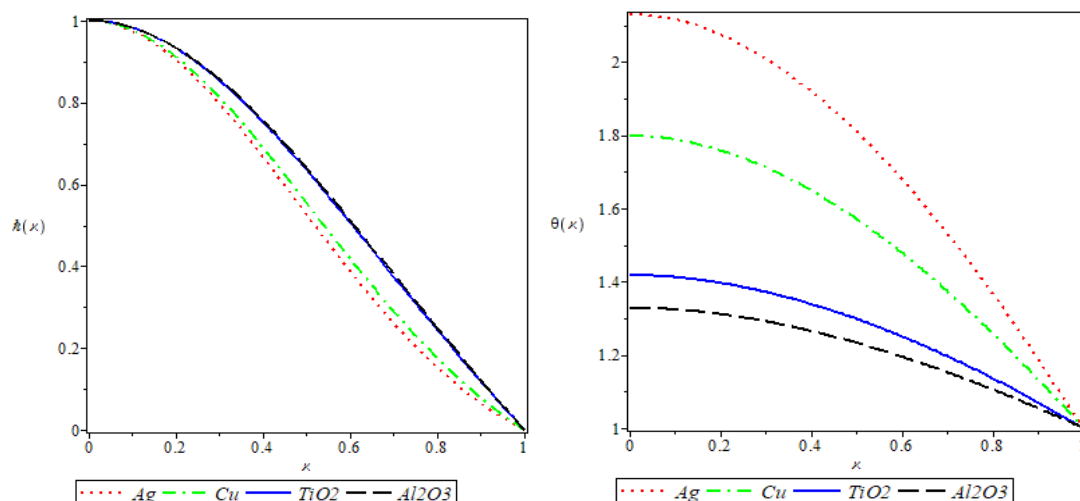


**Figure 7:** Normalized velocity profile and Normalized temperature for three types nanoparticles nanofluid when  $\Re = 50$  ,  $\gamma = 5^\circ$  ,  $E_c = 0.5$  .

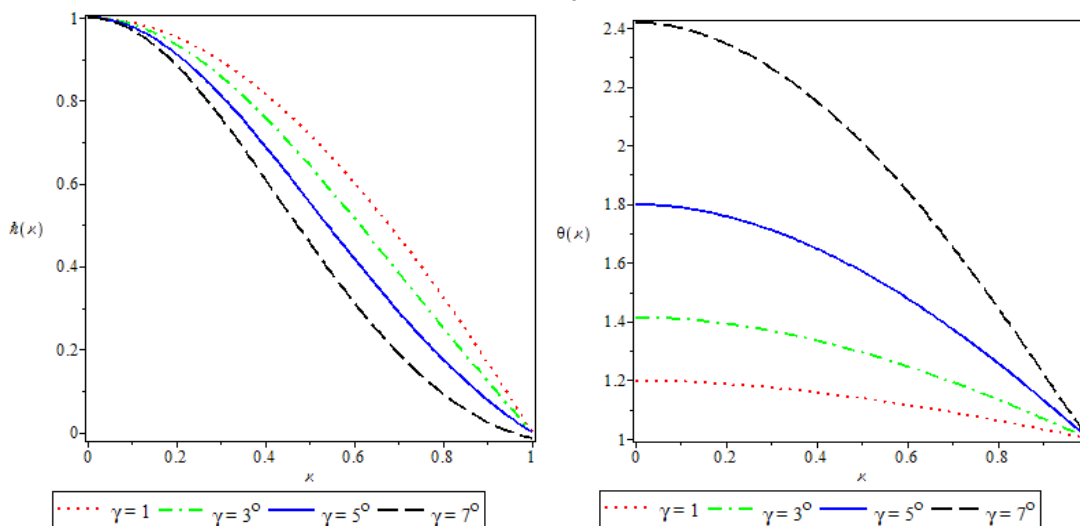


**Figure 8:** Normalized velocity profile and Normalized temperature for Cu nanoparticle nanofluid when  $\Re = 50$  ,  $\phi = 0.2$  ,  $E_c = 0.5$

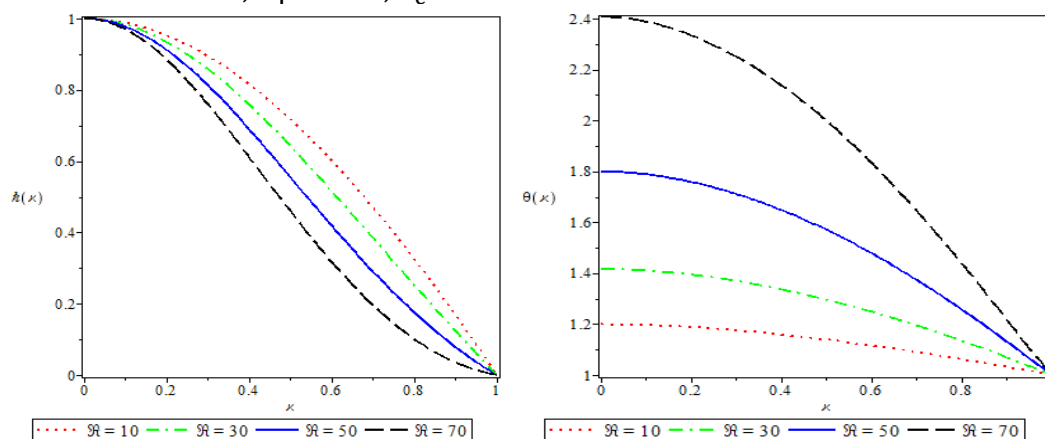


**Figure 9:** Normalized velocity profile and Normalized temperature for Cu nanoparticle nanofluid when  $\gamma = 5$  ,  $\phi = 0.2$  ,  $Pr = 0.01$  ,  $E_c = 0.5$ .

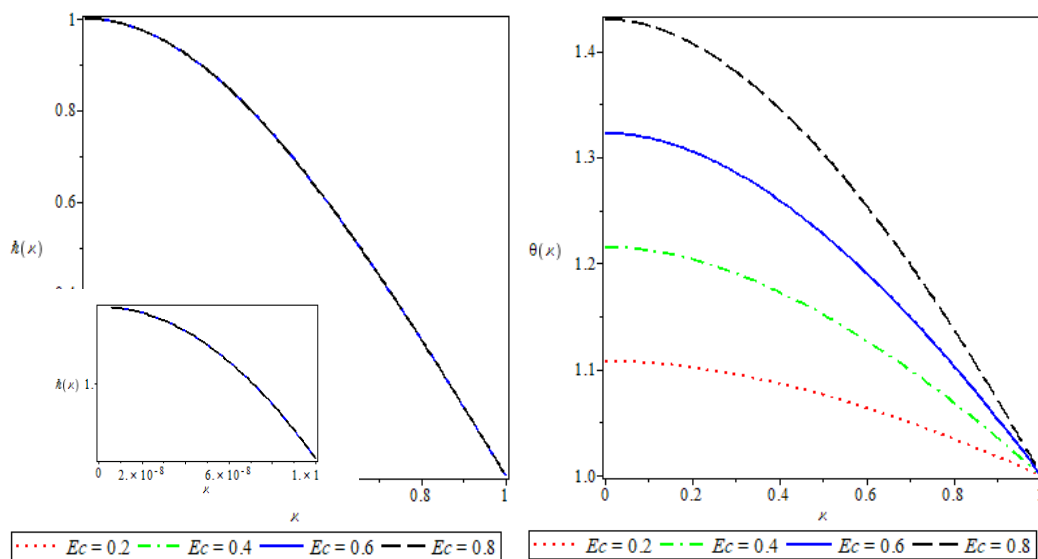


**Figure 10:** Normalized velocity profile and Normalized temperature for Cu nanoparticle nanofluid when  $\gamma = 3$  ,  $\phi = 0.2, Pr = 0.01$  ,  $\mathcal{R} = 30$ .

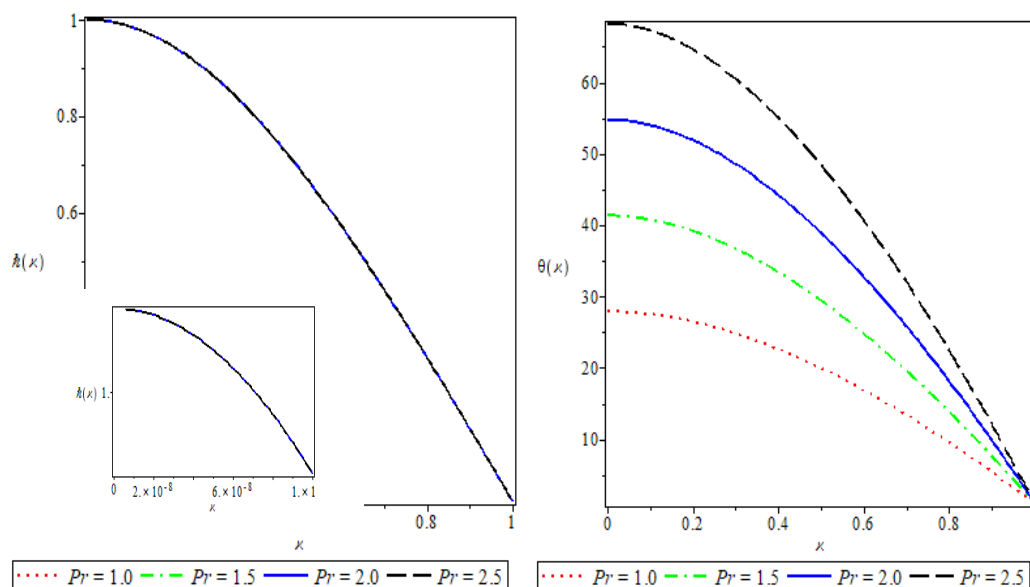


**Figure 11:** Normalized velocity profile and Normalized temperature for Cu nanoparticle nanofluid when  $\gamma = 3$  ,  $\phi = 0.2, Ec = 0.5$  ,  $\mathcal{R} = 30$

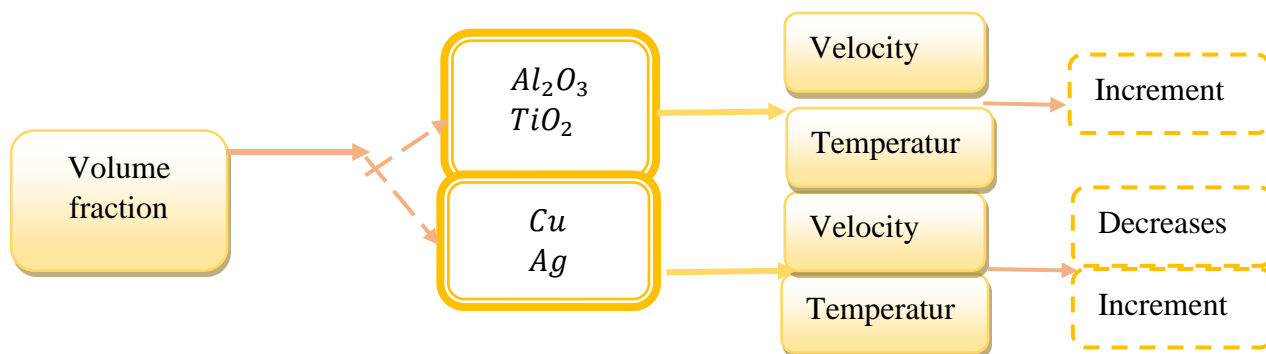


**Figure 12:** The normalized velocity and temperature characteristics of four types of nanoparticle materials with various volume fractions.

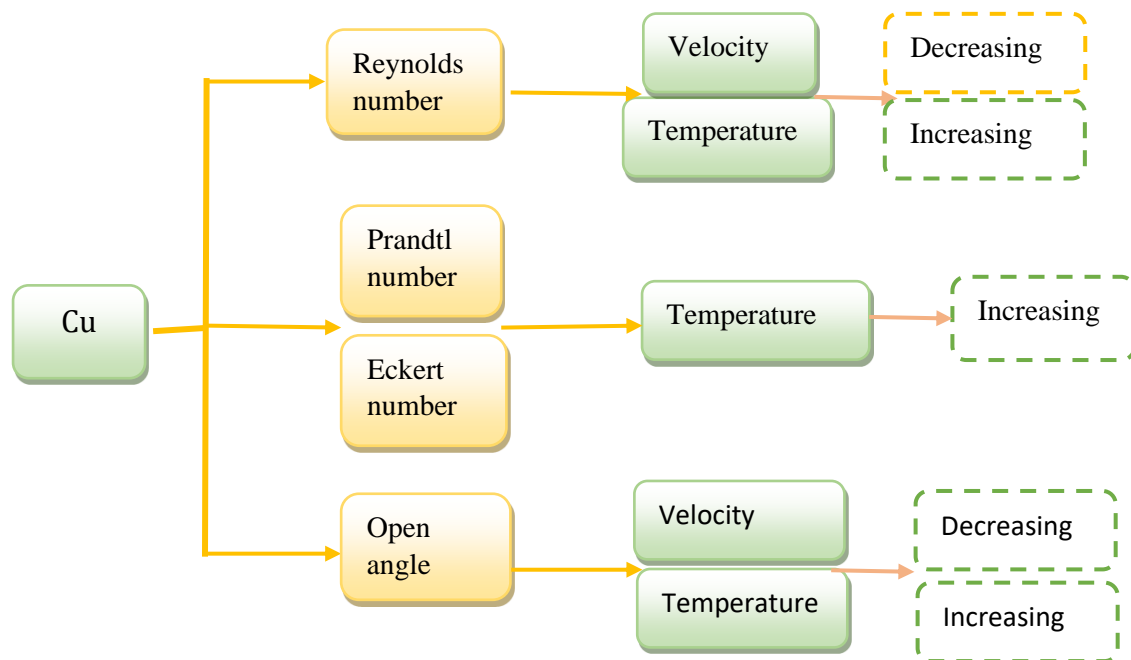


**Figure 13:** The normalized velocity and temperature characteristics of nanoparticle Cu.

## 5. Conclusion

In this work, the impacts of heat transfer on the Jeffery-Hamel nanofluid flow have been discussed. The collected findings demonstrate that PIS is an extremely handy, convenient, practical tool and strategy for obtaining a very precise solution to nonlinear problems. Furthermore, the obtained solutions utilizing the proposed methodology are compared to the approaches HPM, SHAM, and OHAM. The PIS findings show a high level of agreement with numerical values. This way gives new solutions that start with imposing new initial conditions with more constants to get results that have clear convergence and high accuracy which can be noticed when compared with other numerical methods that were previously studied on the same model in previous literature. Figures depict the behavior of the fluid velocity and normalized temperature curves resulting from changes in the physical parameters for various nanoparticle materials Ag, Cu, Al<sub>2</sub>O<sub>3</sub> and TiO<sub>2</sub> in Figures 12 and 13. The future study of this method is done by expanding the horizons of working on nanofluids by taking fluids with higher densities. For example, we can replace water with oil or alcohol, or a mixture between oil and water, and so on with different nanoparticles to obtain a more complex fluid and an advanced issue that can be used in various fields.

## Reference

- [1] L. Rosenhead, "the study two-dimensional radial flow of viscous fluid between two inclined plane walls," *proc.Roy. Sou A*, pp. 436-467, 1940.
- [2] L. M. A. P. E. a. G. A. O. Mahian, "Recent in modeling and simulation of nanofluid flow-Part I:Fundamental and theory," *physics reborts*, vol. 790, no. 3, pp. 1-48, 2019.
- [3] M. G. Sobamowo, "Free convection flow and heat transfer of nanofluids of different shapes of nano-sized particles over a vertical plate at low and high Prandtl numbers," *Applied and Computational Mechanics*, vol. 5, no. 1, pp. 13-39, 2019.

- [4] P. S. a. A. J. C. P. S. Reddy, "Magnetohydrodynamic(MHD) boundary layer heat and mass transfer characteristics of nanofluid over a vertical cone under convective boundary condition," *Propulsion and Power Research*, vol. 7, no. 4, pp. 308-319, 2018.
- [5] A. H. a. M. K. S. Nadeem, "HAM solutions for boundary layer flow in the region of the stagnation point towards a stretching sheet," *Commun Nonlinear Sci Numer Simul*, vol. 15, pp. 81-475, 2010.
- [6] S. S. a. I. U. A. B. Jafar, "MHD radiative nanofluid flow induced by a nonlinear stretching sheet in a porous medium," *Heliyon*, vol. 6, no. 6, 2020.
- [7] N. A. K. F. N. ., M. A. Z. R. a. Q. R. A. Ara, "Numerical simulation for Jeffery-Hamel flow and heat transfer of micropolar fluid based on differential evolution algorithm," *AIP Advances*, vol. 8, no. 1, 2018.
- [8] M. Q. M. M. a. A. J. M. Pourabdian, "The Jeffery-Hamel Flow and Heat Transfer of Nanofluids by Homotopy Perturbation Method and Comparison with Numerical Results," *The 13th Iranian Aerospace Society Conference Faculty of New Sciences and Technologies. University of Tehran*, vol. 65, pp. 135-430, 2014.
- [9] M. E. a. D. D. Ganji, "Solution of Jeffery-Hamel flow problem by optimal homotopy asymptotic method," *Comp. Math. Appl.*, vol. 59, pp. 3405-3411, 2010.
- [10] P. S. F. G. A. a. S. S. S. S. Mosta, "A new spectral homotopy analysis method for the MHD Jeffery-Hamel flow problem," *Computer and Fluids*, vol. 39, pp. 1219-1225, 2010.
- [11] A. M. a. M. F. G. Domairy, "The application of homotopy analysis method to solve nonlinear differential equation governing Jeffery-Hamel flow," *Comm. Nonlinear Sci. Numer. Simulat*, vol. 14, pp. 85-95, 2008.
- [12] a. A. M. J. A. J. Alsaif, "Analytical Investigation of the MHD Jeffery-Hamel flow through convergent and divergent channel by new scheme," *Engineering Letters*, vol. 27, no. 3, pp. 3-28, 2019.
- [13] A. M. J. a. A. J. Alsaif, "New Analytical Solution Formula for Heat Transfer of Unsteady Two-Dimensional Squeezing Flow of a Casson Fluid between Parallel Circular Plates," *Advanced Research in Fluid Mechanics and Thermal Sciences* , vol. 64, no. 2, pp. 219-243, 2019.
- [14] A. M. Jasim, "Analytical approximation of the first grade MHD squeezing fluid flow with slip boundary condition using a new iterative method," *Heat transfer*, pp. 1-21, 2020.
- [15] A. M. Jasim, "New analytical study for nanofluid between two non-parallel plane walls," *Appl. Comput. Mech.*, vol. 7, no. 1, pp. 213-224, 2021.
- [16] A. M. Jasim, "Mean Square Analytical Solution for Beta Statistical Function," *Physics*, pp. 1-13, 2020.
- [17] P. G. D. A. McAlpine, "On the spatio-temporal development of small perturbations of Jeffery-Hamel flows," *Fluid Dynamic Research*, vol. 22, no. 3, pp. 123-138, 2008.
- [18] A. R. a. E. A. Q. Esmaili, "An approximation of the analytical solution of the JefferyHamel flow by decomposition method," *Phys. Letter A*, vol. 372, pp. 3434-3439, 2008.
- [19] P. Y. M. O. D. Makinde, "Hermite-Pade approximation approach to MHD Jeffery-Hamel flows," *Appl. Math. Comput.*, vol. 181, pp. 966-972, 2006.
- [20] F. M.-O. M. R. S. a. B. M. A. S. Hamrelaine, "Analysis of MHD Jeffery Hamel Flow with Suction/Injection by Homotopy Analysis Method," *Advanced Research in Fluid Mechanics*, vol. 59, pp. 173-186, 2019.
- [21] J. H. H. a. E. O. Yusry, "Homotopy perturbation method with three expansions," *mathematical chemistry*, vol. 59, pp. 1139-1150, 2021.
- [22] N. N. F. O. H. a. E. A.-N. T. Mahalakshmi, "Natural convective heat transfer of Ag-water nanofluid flow inside enclosure with center heater and bottom heat source," *Chinese journal of physics*, vol. 56, no. 4, pp. 1497-1507, 2018.
- [23] A. J. H. A. S. J. Al-Saif, "Perturbation-iteration algorithm for solving heat and mass transfer in the unsteady squeezing flow between parallel plates," *Applied and Computational Mechanics*, vol. 5, no. 4, pp. 804-815, 2019.

- [24] S. M. a. R. C. R. L. Bougoffa, "Exact and Approximate Analytic Solutions of the Jeffery-Hamel Flow Problem by the Duan-Rach Modified Domain Decomposition Method," *Mathematical Modelling and Analysis*, vol. 21, no. 2, pp. 174-187, 2016.
- [25] S. L. B. B. R. N. a. K. Petros, "Machine Learning for Fluid Mechanics," *Annual review of fluid mechanics*, vol. 52, pp. 477-508, 2020.
- [26] I. M. A. F. a. J. H. Dehghani, "Improved homotopy perturbation method for geometrically nonlinear analysis of space trusses," *Applied Sciences (Switzerland)*, vol. 10, no. 8, 2020.
- [27] A. S. M. S. H. Abd, "Solving Nonlinear Boundary Value Problem Arising of Natural Convection Porous Fin by Using the Haar Wavelet Collocation Method and Temimi and Ansari Method," *Iraqi Journal of Science*, vol. 63, no. 8, pp. 3592-3599, 2020.
- [28] A. M. A. B. A. Almusawi, "Heat transfer analysis and magnetohydrodynamics effect on peristaltic transport of ree-eyring fluid in rotating frame," *Iraqi Journal of Science*, vol. 62, no. 8, pp. 2714-2725, 2021.
- [29] B. K. a. N. M. R. Sumithra, "The onset of Darcy–Brinkman–Rayleigh–Benard convection in a composite system with thermal diffusion," *Heat Transfer*, vol. 51, no. 1, pp. 604-620, 2022.
- [30] R. S. a. R. K. V. N. Manjunatha, "Influence of constant heat source/sink on non-darcian-Bernard double diffusive Marangoni convection in a composite layer system," *Appl. Math. and Informatics*, vol. 40, no. 2, pp. 99-115, 2022.
- [31] R. . S. N. Manjunatha, "Effects of heat source/sink on darcian-B' Enard-magneto-Marangoni convective instability in a composite layer subjected to nonuniform temperature gradients," *Appl.Math and informatics*, vol. 40, no. 1-2, pp. 99-115, 2022.